J Appl Electrochem (2009) 39:2453–2459
DOI 10.1007/s10800-009-9934-y

ORIGINAL PAPER

# Turbulent fluid flow and electrochemical mass transfer in an annular duct with an obstruction

**G. Weyns · G. Nelissen · J. G. A. Pembery · P. Maciel · J. Deconinck · H. Deconinck · M. A. Patrick · A. A. Wragg**

Received: 3 January 2007 / Accepted: 18 May 2009 / Published online: 2 June 2009


**Abstract** A so-called blockage geometry consisting of a rod with a fin positioned concentrically within a pipe is used to asses the capabilities of numerical turbulent flow and mass transfer models to predict the turbulent mass transfer coefficients. Measurements of the mass transfer coefficient have been performed for a range of fin diameters and flow rates. The limiting diffusion current measurements were performed using the ferri-ferrocyanide system and nickel electrodes. Different mass transfer turbulence models are used for the calculations and the results are compared with the measurements. The influence of flow rate and fin diameter on the mass transfer rate is examined.

G. Weyns (✉) · G. Nelissen · P. Maciel · J. Deconinck
Vakgroep Elektrotechniek, Vrije Universiteit Brussel,
Pleinlaan 2, 1050 Brussels, Belgium
e-mail: gweyns@vub.ac.be

G. Nelissen
Elsyca NV, Vaartdijk 3, 3018 Wijgmaal, Belgium

J. G. A. Pembery
Flowmasters Ltd., The Maltings, Pury Hill Business Park,
Alderton Road, Towcester NN12 7TB, UK

H. Deconinck
von Karman Institute for Fluid Dynamics,
Waterloosesteenweg 72, 1630 Sint-Genesius-Rode, Belgium

M. A. Patrick
Institut Catholique d'Arts et Metiers, 6 rue Auber,
59046 Lille Cedex, France

A. A. Wragg
Department of Engineering, University of Exeter,
Exeter EX4 4QF, UK

**Keywords** Blockage geometry · Fins · Mass transfer coefficient · Turbulent mass transfer · Limiting current

**List of symbols**

| | |
|---|---|
| $c_b$ | Bulk concentration of the reacting ion, mol $m^{-3}$ |
| $c_k$ | Concentration of species k, mol $m^{-3}$ |
| $c_s$ | Surface concentration of the reacting ion, mol $m^{-3}$ |
| $d_e$ | Equivalent diameter of duct, m |
| $d_i$ | Diameter of the rod, m |
| $D$ | Molecular diffusion constant of reacting ion, $m^2\ s^{-1}$ |
| $D_k$ | Molecular diffusion constant of species k, $m^2\ s^{-1}$ |
| $d_o$ | Outside diameter of the annulus, m |
| $D_t$ | Turbulent diffusion coefficient, $m^2\ s^{-1}$ |
| $F$ | Faraday constant, 96,487 °C $mol^{-1}$ |
| $i$ | Current, A |
| $i_{lim}$ | Limiting current, A |
| $k_m$ | Mass transfer coefficient, m $s^{-1}$ |
| $L^+$ | Dimensionless length of the cathode |
| $L_{tot}$ | Length of the cathode, 0.1 m |
| N | Mass transfer rate (ion flux), mol $s^{-1}$ |
| $Re$ | Reynolds number |
| $S$ | Area of the electrode, $m^2$ |
| $Sc$ | Schmidt number |
| $Sc_t$ | Turbulent Schmidt number |
| $Sh$ | Sherwood number |
| $Sh_{CC}$ | Sherwood number obtained from the Chilton-Colburn correlation |
| $y$ | Normal distance to the wall, m |
| $y^+$ | Dimensionless normal distance to the wall, as defined in [19] |
| $z$ | Charge of reacting ion |
| $\bar{u}$ | Velocity vector, m $s^{-1}$ |

**Greek**

| | |
|---|---|
| $\mu$ | Dynamic viscosity, kg $m^{-1}$ $s^{-1}$ |
| $\nu$ | Kinematic viscosity, $m^2$ $s^{-1}$ |
| $\nu_t$ | Turbulent viscosity, $m^2$ $s^{-1}$ |
| $\tau_{wall}$ | Surface shear stress, kg $m^{-2}$ $s^{-2}$ |

## 1 Introduction

A wide range of investigations have been performed on blockage geometries by various workers such as Chapman [21], Ihle et al. [22], Davis [23], Hall and Duffey [24], Cadek et al. [25], Hall et al. [26] and many others. The investigation of such geometries is essential in design and safety studies to understand how ballooning of fuel rod cladding might affect the subsequent thermal history of a Pressurized Water Reactor which has suffered a loss-of-coolant accident.

Pembery provides experimentally determined mass transport coefficients for a variety of blockage geometries [4, 28, 29]. Four geometries are examined: axisymmetric fins, an axisymmetric bulged rod, a necked tube and a rod cluster. Data of Pembery for the axisymmetric fin case is used here to assess the capabilities of turbulent flow and mass transfer models to predict the turbulent mass transfer coefficients.

In Pembery's work, undertaken at Exeter University, UK, measurements of mass transfer coefficient were carried out for a range of fin diameters and flow rates. The limiting diffusion current measurements were performed using the ferri-ferrocyanide electrochemical system using local nickel electrodes embedded in an active surrounding electrode.

Different mass transfer turbulence models are used here for the calculations and the results are compared with the earlier measurements. The influence of flow rate and fin diameter on the local mass transfer rate is examined.

## 2 Geometry of the pipe with an obstruction

The geometry under consideration is an axisymmetric nickel rod with an inert PVC fin positioned concentrically within a nickel pipe, thus producing an annular duct. A detailed description of the geometry, the flow conditions and the electrochemical measurement equipment and techniques can be found in [4]. The pipe formed the outside surface of the annular channel. The diameter of the rod was 12 mm and the inner diameter of the pipe was 51.8 mm. A schematic representation of the rod is given in Fig. 1a.

The actual shape of the fin is shown in Fig. 1b. For the calculations, only the geometry with an outer fin diameter of 32 mm was used. In the experiments, four different fin diameters were used, 27, 32, 37 and 42 mm.

The 32 flush mounted mini-electrodes were made from a 99.99% pure 1 mm nickel wire and were positioned 12.5 mm apart in 1.4 mm holes in the nickel rod. The mini electrodes were insulated from the main electrode to permit local measurement of current to be made and point mass transfer coefficients to be determined. Araldite insulation was used to insulate and isolate the mini electrodes from the main cathode rod. This insulation gap between the two electrodes causes the mass transfer boundary layer to dissipate over the small inactive region. However, it was determined numerically that this effect has a very small effect on the local mass transfer coefficient.

For the electrical connection of the local electrodes 0.2 mm diameter nickel wire was used. The outer surface of the annulus (the pipe) was used as anode.

## 3 Flow for annulus with obstruction

As no flow measurements for this geometry are available, the turbulent flow solver (esp the k–$\omega$ model of Wilcox 2001) has been validated to simulate the flow in a comparable geometry [2, 3, 6, 7]. To this purpose the calculated turbulent flow in a pipe with an axisymmetric expansion has been validated with measurements presented in [5]. A detailed description of the turbulence model is given in [7], while the numerical approach to solve the Navier-Stokes equations and the turbulence equations is presented in [27]. The general agreement between the calculation and the experimental values of the velocity and turbulent kinetic energy profiles is good. However, the size of the main recirculation zone is overestimated by about 35%.

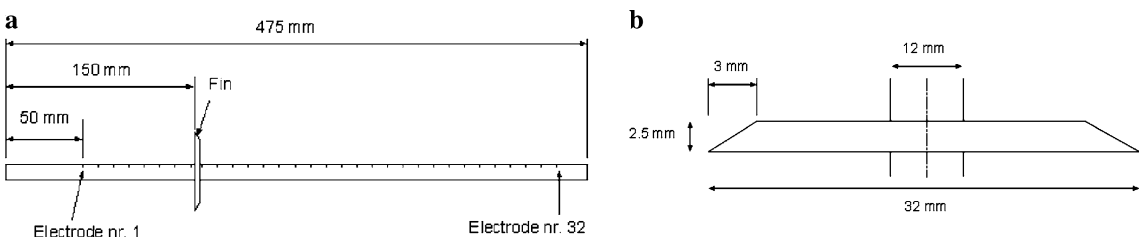


**Fig. 1** **a** Schematic drawing of the rod with the fin. **b** Schematic drawing of the fin

The Reynolds number is defined on the basis of the mean inlet velocity and the equivalent diameter, case equal to:

$$d_e = d_o - d_i. \quad (1)$$

For the geometry under consideration here the equivalent diameter is 39.8 mm.

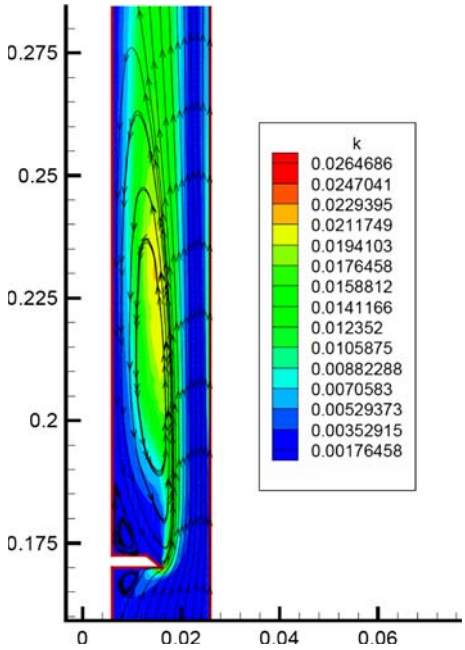


**Fig. 2** Overview of the flow and the kinetic energy, $Re = 13{,}200$, dimensions in m

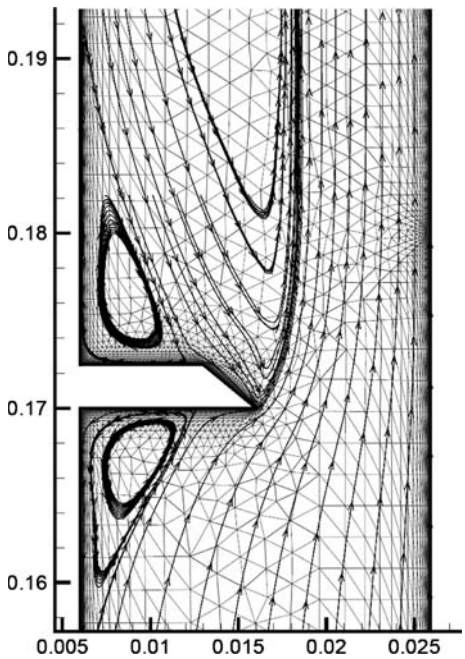


**Fig. 3** Detail of the flow and the mesh near the fin, $Re = 13{,}200$, dimensions in m

The streamlines and turbulent kinetic energy for $Re = 13{,}200$ and a fin diameter of 32 mm are shown in Fig. 2. The streamlines and the grid near the fin are represented in Fig. 3. There are three recirculation zones visible in Fig. 2: one in front of the fin, one big recirculation zone behind the fin and a third smaller recirculation zone beneath the second close to the fin as determined and described by Tagg et al. [30].

## 4 Measurements

Various electrochemical systems can be used to obtain limiting currents. To avoid deposition reactions that would roughen the surface of the electrode and thus influence the flow and surface area, the ferri-ferrocyanide system is often chosen. The reaction taking place at the cathode is:

$$Fe(CN)_6^{3-} + e^- \leftrightarrow Fe(CN)_6^{4-}. \quad (2)$$

As the opposite reaction occurs at the anode, there is no net production or consumption of ions; hence the concentration of all species remains constant over time.

When using the ferri-ferrocyanide system, ferricyanide reduction at the cathode is employed as the limiting reaction because it gives a better limiting current plateau than the anodic reaction [4]. The cathodic reaction involves a species with a higher diffusivity than the anodic reaction and therefore the anode has to be bigger than the cathode in order to achieve limiting conditions at the cathode. The diffusion coefficient D of the ferricyanide ion is $6.631 \times 10^{-10}$ m$^2$ s$^{-1}$ at 20 °C, leading to a Schmidt number of 1,632. The electrolyte consists of 0.005 M equimolar mixture of potassium ferri- and ferrocyanide with a supporting electrolyte of 0.5 M sodium hydroxide. The large amount of supporting electrolyte ensures that the effects of migration on the transport of reacting ions are negligible.

The density of the ferri-ferrocyanide/NaOH electrolyte is 1,020.5 kg m$^{-3}$ and the dynamic viscosity is $1.105 \times 10^{-3}$ N s m$^{-1}$ at 20 °C [4].

The aim of the experiments is to obtain the local mass transfer coefficient along the rod. The mass transfer coefficient $k_m$ is defined as:

$$N = \frac{i}{zF} = k_m S(c_b - c_s). \quad (3)$$

For the limiting current situation, the concentration of the reacting ion is equal to zero at the electrode, $c_s = 0$. Therefore, the mass transfer is related to the limiting current ($i_{lim}$) via:

$$k_m = \frac{i_{lim}}{zFc_b S}. \quad (4)$$

This means that the local mass transfer coefficient can be computed from measurements of the local limiting current. As the local limiting current is an integral quantity, the mass transfer coefficient will be a (local) mean value. The local limiting current density along the rod is measured at the mini-electrodes. Using Eq. 3 this local current density is transformed into a local mass transfer coefficient.

The values of the mass transfer coefficient for a fully developed turbulent flow in an annular geometry are given by a correlation from Berger and Hau as reported in [4], which for Schmidt numbers larger than 1,000 is:

$$Sh = \frac{k_m d_e}{D} = 0.0165 Re^{0.86} Sc^{0.33}. \quad (5)$$

Additionally, Baehr [1] reports the following correction to the Chilton-Colburn correlation for turbulent mass transfer in an annular duct:

$$Sh = 0.86 \left(\frac{d_i}{d_o}\right)^{-0.16} Sh_{CC} \quad (6)$$

with $Sh_{CC}$ the Sherwood number obtained from the Chilton-Colburn correlation as given in

$$Sh = 0.023 Re^{0.8} Sc^{1/3}. \quad (7)$$

This correction assumes that only the inner surface (the rod in this case) is used to perform the mass transfer measurements. For comparison purposes, these two correlations, labeled 'Berger and Hau' and 'Chilton-Colburn' are shown in the figures for the mass transfer coefficient along the rod.

## 5 Modelling mass transfer in turbulent flow

### 5.1 Turbulent mass transfer

When migration is neglected, the steady state convection-diffusion equation can be written as

$$\bar{u}\bar{\nabla} c_k = \bar{\nabla}(D_k \bar{\nabla} c_k). \quad (8)$$

Similar to modelling turbulent fluid flow, the effects of turbulence on mass transfer are modelled by adding the turbulent diffusion $D_t$ to the molecular diffusion:

$$\bar{u}\bar{\nabla} c_k = \bar{\nabla}[(D_k + D_t)\bar{\nabla} c_k]. \quad (9)$$

For mass transfer the following dimensionless numbers are commonly used:

$$Sc = \frac{v}{D} \quad (10)$$

the Schmidt number, equivalent to the Prandtl number in heat transfer, describing the ratio between the viscosity and the molecular diffusion and

$$Sc_t = \frac{v_t}{D_t} \quad (11)$$

the turbulent Schmidt number, equivalent to the turbulent Prandtl number, describing the ratio between the turbulent viscosity and the turbulent diffusion.

### 5.2 Turbulence models for mass transfer

Several models have been proposed [8–10, 12–16] to calculate turbulent diffusion. The influence of different turbulent mass transport models on the predicted limiting current have been investigated by Nelissen et al. [27]. Most of these models are straightforward extrapolations of models for turbulent heat transfer [12]. However, because the mass transfer boundary layer is at least one order of magnitude smaller than the hydrodynamic and thermal boundary layers, this similarity does not always hold.

The models used here are:

- $D_t = 0$. The turbulent diffusion is neglected because it is assumed that the turbulent boundary layer is so small that all the effects happen in the laminar sublayer of the turbulent fluid flow. This assumption is valid if the length of the electrode is small [18] $\left(L_{tot}\sqrt{\tau_{wall}/\mu\nu} = L^+ < 700\right)$.
- $D_t \propto v_t$ or $Sc_t$ = constant. This is the straightforward extrapolation to mass transfer of what is generally done in turbulent heat transfer [11, 17]. A typical value for the constant is 0.71. More elaborate models consider

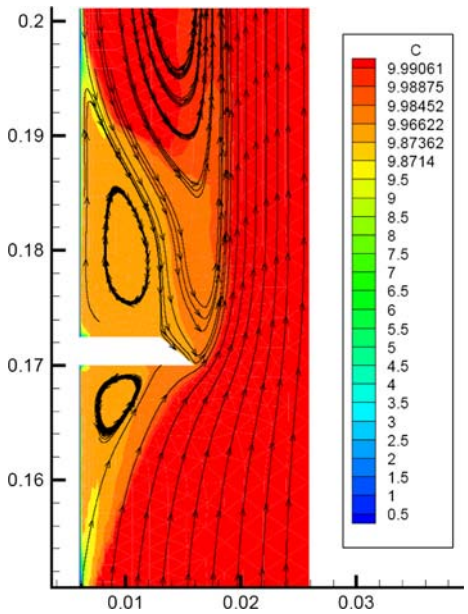


**Fig. 4** Concentration distribution near the fin, $Re$ = 6,400, dimensions in m

the dependence of $Sc_t$ on some global quantities of the flow (Re, Sc, boundary layer thickness, …) [13].

- $D_t$ is given by an algebraic turbulence model. This is the equivalent of an algebraic turbulence model for flow. Several different models have been developed [8, 12, 19, 20], most of them based on one set of measurements. Most models start from the fact, both theoretical and experimental, that the turbulent diffusion varies with $y^3$ close to the wall. A typical example is the model proposed by Aravinth [12]:

$$\frac{D_t}{\nu} = \frac{0.0007y^{+3}}{(1+0.00405y^{+2})^{0.5}}, \quad 0<y^+<30,\ Sc\geq 1. \qquad (12)$$

## 6 Calculations

The flow field as shown in Sect. 3, is interpolated to a grid specially refined for mass transfer calculations. As only the linear convection-diffusion equation is solved, machine accuracy is achieved in two iterations.

Figure 4 shows the concentration distribution and the streamlines of the flow in the region near the fin for $Re = 6{,}400$. Again a very small mass transfer boundary layer is observed. The direct influence of the flow, especially the recirculation zones, on the concentration distribution is clearly noticeable.

### 6.1 Influence of turbulence model

In Fig. 5 the mass transfer coefficient along the rod is shown for $Re = 24{,}150$ calculated using different turbulent mass transfer models. On the $x$-axis the distance from the leading edge of the fin is used. From this it is clear that the electrode length is not long enough to exhibit a big difference between the turbulence models. As long as the turbulent mass transfer boundary layer remains small molecular diffusion is dominant and thus the resulting turbulent mass transfer remains independent of the model chosen for the turbulent diffusion. Only near the end of the electrode is a small difference noticeable. The model $Sc_t = 1$ overestimates the turbulent diffusion coefficient, while $D_t = 0$ underestimates the mass transfer coefficient. Both the algebraic model and the model $Sc_t = 4.5$ yield almost exactly the same results between the two extremes mentioned above.

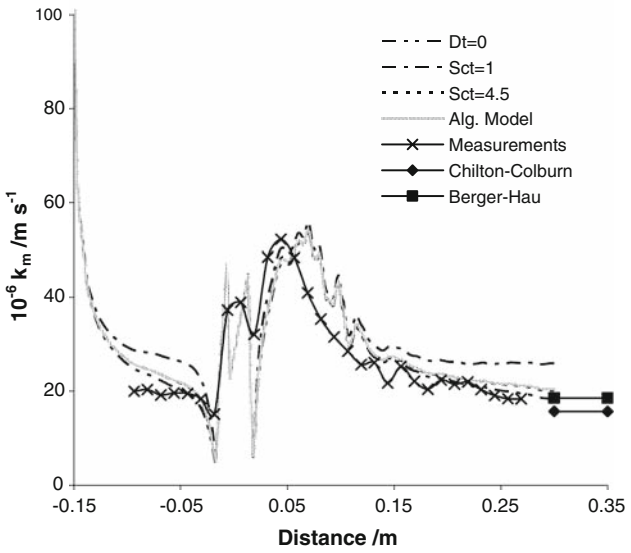


**Fig. 5** Mass transfer coefficient distribution along the rod, $Re = 24{,}150$

The general trend of the calculated mass transfer coefficient distribution and the measured values matches very well.

In both the experiments and the calculations, the electrode starts 50 mm before the first measuring point (mini-electrode). The measurements indicate that this is sufficient to have a complete developed mass transfer boundary layer, while the calculations suggests that there is still a big variation in the mass transfer coefficient for the first group of measuring points. Simulations were performed imposing $c = 0$ at the electrode, which is numerically equal to imposing the limiting current, whereas in the experiments a potential is applied which yield the limiting current. At the part of the electrode closest to the inlet, the assumption $c = 0$ causes a very high peak in current density in the simulations, as confirmed by the Leveque solution [31] which shows that the mass-transfer rate becomes infinite near the beginning of the mass-transfer section. This phenomenon is not found in the experiments because the first mini-electrode is 50 mm downstream of the start of the electrode. However, this effect might be overestimated by the simulations because the recirculation zone upstream of the fin is not well predicted. It is also possible that this initial effect is not correctly captured in the experiments due to the fact that the entire electrode is not operating at limiting current density. In reference [32] it is shown that when 97% of the limiting current is imposed, the concentration over a portion on the upstream side of the electrode can be significantly different from zero. This then means that the numerical boundary condition does not correspond to the measured reality in the upstream part of the electrode.

As expected from the flow calculations for a pipe expansion [5], the length of the main recirculation zone downstream of the fin is overestimated. This is indicated by the fact that the point where the mass transfer is maximum is further downstream than the measured peak in the mass transfer coefficient. However, the absolute value of the peak mass transfer coefficient matches perfectly between measurements and simulations. The peak in the mass transfer coefficient directly behind the fin is due to the second

recirculation zone. This peak is not present in the measurements because the spacing between the point electrodes is too large. The size of the recirculation zone upstream of the fin is captured almost perfectly.

Far downstream from the fin fully developed mass transfer coefficients are found both in the measurements and in the simulations. The best agreement is reached for the algebraic model and the model $Sc_t = 4.5$.

The small oscillations and secondary peaks for the calculated mass transfer coefficient are caused by the implemented LDA scheme [33].

Figure 6 shows the mass transfer coefficients along the rod for different turbulence models for $Re = 6{,}400$. The same conclusions concerning the position and value of the peaks in the mass transfer coefficient are valid as for $Re = 24{,}000$. However, for this flow rate the influence of the turbulence models is almost negligible, showing that the influence of the turbulent diffusion in small compared to the molecular diffusion. Also the mass transfer coefficient for a fully developed flow is found most accurately when using the algebraic model and the model $Sc_t = 4.5$.

## 6.2 Influence of flow rate

Figure 7 represents the calculated and measured mass transfer coefficients for $Re = 6{,}400$, $Re = 13{,}200$ and $Re = 24{,}150$. For each of these calculations the model $Sc_t = 4.5$ is used. Overall, the trend of the calculations and the measurements agrees well for all flow rates. The higher the flow rate, the better the calculations and measurements match, especially concerning the position of the peak value of mass transfer coefficient.

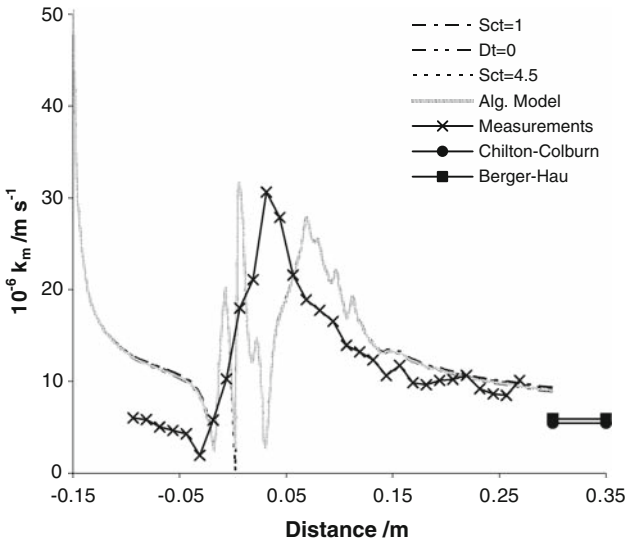


**Fig. 6** Mass transfer coefficient distribution along the rod, $Re = 6{,}400$

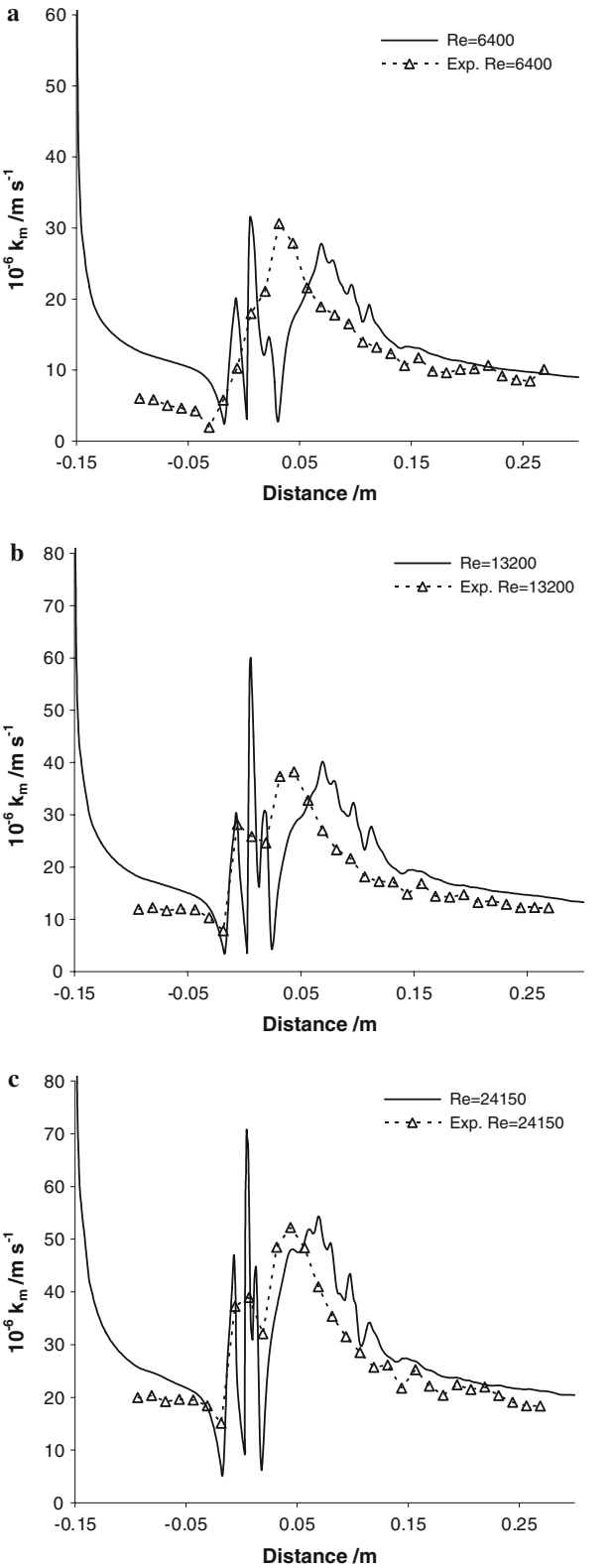


**Fig. 7** **a** Mass transfer coefficient distribution along the rod for $Re = 6{,}400$. **b** Mass transfer coefficient distribution along the rod for $Re = 13{,}200$. **c** Mass transfer coefficient distribution along the rod for $Re = 24{,}150$

The very strong variation in the calculated values of the mass transfer coefficient near the fin is due to the complex structure of the smaller recirculation zone(s) directly in front and behind the fin.

As noted from experiments [4], the position of the peak in the mass transfer coefficient profile increases slowly in the downstream direction with Reynolds number. This trend is not found in the numerical simulations, as the position of the peak mass transfer is almost independent of the flow rate. Again this is of course related to the problems encountered by the k–$\omega$ model to predict the recirculation zone length accurately for different flow rates and configurations.

## 7 Conclusions

The turbulent mass transfer coefficient in an annular duct with an obstruction on the inner core has been calculated using different turbulent mass transfer models. The results are compared with earlier measurements obtained from limiting current experiments using the ferri-ferrocyanide system. Also correlations for fully developed mass transfer are used to validate the calculations. The qualitative and the quantitative agreements between calculations and measurements are good, except for the position of the peak in the mass transfer profile. As this peak is related to the recirculation zone length, the position of the peak is overestimated (as expected), because the flow solver also produced this result in other comparable geometries. Also the influence of the flow rate is predicted correctly by the simulations. Far downstream of fin, the mass transfer coefficient for fully developed flow is obtained.

It can be concluded that, although not perfect, these results prove that the numerical models provide very acceptable predictions of turbulent mass transfer suited to industrial applications.

**Acknowledgements** This research was funded by FWO-Vlaanderen under contract number G.0091.05, by the European Commision under contract number 216474 and by the UKAEA, Winfrrith.

## References

1. Baehr HD (1994) Warme-und Stoffubertragung, 3rd edn. Springer Verlag, Berlin
2. Kral LD (1998) Prog Aerosp Sci 34:481
3. Menter FR (1994) Am Inst Aeronaut Astronaut J 32:1598
4. Pembery JGA (1985) Mass transfer modelling of heat transfer in partially blocked nuclear fuel bundles. PhD thesis, University of Exeter
5. Stieglmeier M, Tropea C, Weiser N, Nitsche W (1989) J Fluids Eng 111:464
6. Waterson N (2003) Flow simulation at low Mach number using a residual-distribution approach. PhD thesis, Technische Universiteit Delft
7. Wilcox DC (1998) Turbulence modeling for CFD, 2nd edn. DCW Industries, CA
8. Notter RH, Sleicher A (1971) Chem Eng Sci 26:161
9. Reynolds AJ (1975) Int J Heat Mass Transf 18:1055
10. Churchill SW (1997) Ind Eng Chem Res 36:3866
11. Wang Y, Postlethwaite J (1997) Corros Sci 39:1265
12. Aravinth S (2000) Int J Heat Mass Transf 43:1399
13. Rosen C, Traegaardh C (1995) Chem Eng J Biochem Eng J 59:153
14. Chalupa R, Chen M, Modi V, West AC (2001) Int J Heat Mass Transf 44:3775
15. Gurniki F, Fukagata K, Zahrai S, Bark FH (2000) J Appl Electrochem 30:1335
16. Heyerichs K, Pollard A (1996) Int J Heat Mass Transf 39:2385
17. Nesic S, Postlethwaite J, Bergstrom DJ (1992) Int J Heat Mass Transf 35:1977
18. Shaw DA, Hanratty TJ (1977) AIChE J 23:160
19. Martemyanov S, Skurygin E, Legrand J (1999) Int J Heat Mass Transf 42:2357
20. Mizushina T, Ogino F, Oko Y, Fuduka H (1971) Int J Heat Mass Transf 14:1705
21. Chapman RH (1978) Preliminary multirod burst test program results and implications of interest to reactor safety evaluations. 6th Water React Saf Res Inf Meet, Gaithersburg, Maryland
22. Ihle P, Politzky M, Rust K (1980) FEBA—Flooding experiments with blocked arrays—Heat transfer in partly blocked 25-rod bundle. 19th National Heat Transfer Conference, Orlando, Florida
23. Davis PR (1971) Nucl Technol 11:551
24. Hall PC, Duffey RB (1975) Nucl Sci Eng 58:1
25. Cadek FF, Dominicus DP, Leyse RH (1970) PWR FLECHT (Full Length Emergency Cooling Heat Transfer) Group II Test Report. WCAP-7544, Westinghouse Atomic Power Division
26. Hall WB, Ionnov GP, Turner JT (1977) Heat transfer in the vicinity of a partial flow blockage in a reactor core. Conf Proc I Mech E, No 8, 143, Manchester
27. Nelissen G, Weyns G, Maciel P, Deconinck J, Vande Vyver O, Deconinck H (2007) Electrochim Acta 52:6584
28. Pembery JGA, Wragg AA, Patrick MA (1984) Proceedings of the 11th Annual I Chem E Research Meeting, Bath, UK, pp 141–146
29. Patrick MA, Pembery JGA, Wragg AA (1984) Proceedings of the 1st UK Heat Transfer Conference, Leeds, UK, pp 879–892
30. Tagg DJ, Patrick MA, Wragg AA (1979) Trans Inst Chem Eng 57:176
31. Newman J, Thomas-Alyea KA (2004) Electrochemical systems, 3rd edn. Wiley-Interscience, New Jersey
32. Nelissen G, Van Theemsche A, Dan C, Van den Bossche B, Deconinck J (2004) J Electroanal Chem 563:213
33. van der Weide E (1998) Compressible flow simulation on unstructures grids using multi-dimensional upwind schemes